Neutron Bragg-edge-imaging for strain mapping under *in situ* tensile loading

R. Woracek,[1,2] D. Penumadu,[1,a)] N. Kardjilov,[2] A. Hilger,[2] M. Strobl,[2] R. C. Wimpory,[2] I. Manke,[2] and J. Banhart[2]
[1]*University of Tennessee, CEE Department, 223 Perkins Hall, Knoxville, Tennessee 37996, USA*
[2]*Helmholtz Zentrum Berlin, Hahn Meitner Platz 1, D-14109 Berlin, Germany*

(Received 18 November 2010; accepted 22 March 2011; published online 3 May 2011)

Wavelength selective neutron radiography at a cold neutron reactor source was used to measure strain and determine (residual) stresses in a steel sample under plane stress conditions. We present a new technique that uses an energy-resolved neutron imaging system based on a double crystal monochromator and is equipped with a specially developed (*in situ*) biaxial load frame to perform Bragg edge based transmission imaging. The neutron imaging technique provides a viewing area of 7 cm by 7 cm with a spatial resolution on the order of ~ 100 μm. The stress-induced shifts of the Bragg edge corresponding to the (110) lattice plane were resolved spatially for a ferritic steel alloy A36 (ASTM international) sample. Furthermore it is demonstrated that results agree with comparative data obtained using neutron diffraction and resistance based strain-gauge rosettes. © *2011 American Institute of Physics*. [doi:10.1063/1.3582138]

I. INTRODUCTION

Besides traditional neutron imaging (based on attenuation contrast) of materials several additional methods have recently evolved, e.g., phase contrast,[1–3] differential phase contrast,[4–7] dark-field imaging,[8–10] and imaging with polarized neutrons.[11–14] Energy selective neutron imaging opens possibilities to exploit the Bragg-edges of crystalline materials and reveal microstructural information related to the lattice spacing, such as phase, texture and strain.[15,16] Neutron diffraction instruments at spallation sources have been used to investigate the transmission spectrum and the observed Bragg-edge was used for strain mapping.[17–23] A new technique to evaluate elastic strain components, using an established neutron imaging instrument at a reactor source in combination with a monochromator device, will be presented in this paper. The method has the potential to be a powerful tool to perform spatially resolved 2-D phase or strain mapping and opens up possibilities of phase/strain tomography and texture studies as well.[24,25]

The transmission spectrum of neutrons in the thermal to cold energy range through a (poly-) crystalline sample shows a sharp increase at certain wavelengths. The position of these so called "Bragg Edges" is directly related to the lattice spacing d_{hkl}, and therefore the method is suited for strain measurements.[17–19] Compared to the well established diffraction technique, this imaging method can provide data for large areas simultaneously, while measured strains are integrated over the sample thickness. According to Bragg's law,

$$n\lambda = 2d_{hkl}\sin\theta, \tag{1}$$

neutrons at a wavelength λ are coherent-elastically scattered from lattice planes with distances d_{hkl}, which are aligned at an angle θ to the incoming neutron beam, in directions with scattering angles of 2θ. For a particular *hkl*, the scattering angle increases as the wavelength is increased until $2\theta = 180°$ (backscattering toward the source). This is reached at $\lambda = 2d_{hkl}$ and for wavelengths larger than this value, no more scattering from this plane can occur, resulting in a sharp increase of transmitted intensity. Strains can be determined as

$$\varepsilon = (d_{hkl} - d^0_{hkl})/d^0_{hkl} \tag{2}$$

with d^0_{hkl} as the unstrained or reference state lattice parameter.

Several dedicated neutron radiography/tomography instruments at steady state sources can readily provide spatial resolutions on the order of or smaller than 50 μm,[26–29] and therefore implementation of energy selective Bragg-edge imaging techniques could open many new applications. Current improvements at the Helmholtz Zentrum Berlin (HZB) will lead to much higher spatial resolutions using cold neutrons and, therefore, even microstructural features such as phase differences and/or precipitates could possibly be visualized in the future.

In principle there are two possibilities to do such energy dependent measurements at a reactor source: (1) using the time-of-flight information in distance from the source using a specifically designed chopper system or (2) selection (or suppression) of neutrons from specific spectral parts.[30] In the latter case the wavelengths can be selected by a velocity selector, the "slit method" or a wavelength tunable device, e.g., a double crystal monochromator.[15,30,31] Using different settings or crystals allow selection of a very narrow spectral part, but one should keep in mind that the flux decreases as a narrower wavelength band is selected. In this case a double crystal monochromator is used and has been reported previously by Treimer *et al.*[15]

II. EXPERIMENTAL APPROACH

The CONRAD instrument at HZB was used to obtain the location and stress induced shifts of the Bragg-edge corresponding to the (110) lattice plane of a BCC steel sample

a)Electronic mail: dpenumad@utk.edu.

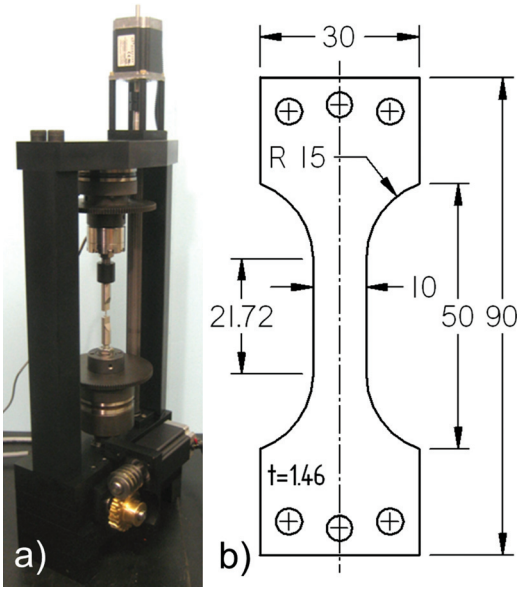

FIG. 1. (Color online) (a) Portable loading system. (b) Specimen dimensions in mm.

(A36 ASTM international) under well-known 2-D stress conditions. A portable mechanical loading system (Fig. 1) has been designed for the purpose of these experiments, specially suited for transmission imaging and tomography. The system offers an axial force capacity of 0–50 kN and a torque range of 0–12 Nm. The system offers a custom developed Graphical User Interface with stress, strain and deformation controls.

Because of the selected sample dimensions (gauge length: 21.72 mm, gauge width: 10 mm, thickness: 1.46 mm; Fig. 1(b)), a 2-D state of stress and hence strain can be assumed. This has been verified calculating the principal strains using a rosette strain gauge and applying uni-axial loading in tension (in z-direction, hence $\gamma_{xy}=0$) and torsion ($\varepsilon_x=\varepsilon_y=0$). Strain in the measured direction using Bragg edge shifts can be therefore attributed purely to Poisson strain. The average grain size of the sample was 25 μm.

The energy selectivity at the CONRAD instruments was achieved by using a double-monochromator consisting of one pyrolytic graphite crystal (PCG) monochromator in the upper and lower position, each with a mosaic spread of 0.8°. The wavelength band has an approximate resolution of $\Delta\lambda/\lambda=3\%$ and can be tuned freely between 2.0 and 6.5 Å while the beam position remains unchanged. The approximate flux at the sample position is 2×10^4 cm^{-1} s^{-1}. The position of the Bragg-edge at $\sim$4.05 Å, corresponding to the (110) lattice plane ($d_{110}=2.02695$ Å), was investigated as it is the most pronounced and the neutron flux is still reasonably high (peak flux at $\sim$3 Å).

Transmission measurements were performed at four different states of stress: (1) unloaded as reference measurement to determine the unstressed lattice parameter d^0_{hkl} (S1) (2) elastic deformation at 90% of yield strength, i.e., 200MPa (S2) (3) plastic deformation (S3), (4) unloaded after previous plastic deformation (S4). (Fig. 2)

The tensile test was performed in deformation (PID) control to not introduce any creep behavior over the measurement time, using a maximum deformation rate of 0.5 mm/min. At each state of stress, 21 transmission measurements between 3.8 and 4.2 Å with a step size of 0.02 Å were performed. The exposure time for each transmission measurement was chosen to be 15 min (+15 min for Flat-field measurement) to minimize signal to noise ratio, resulting in approximately 10.5 hs count time for one stress state. Figure 2 shows the stress-strain curve recorded during the experiment at CONRAD, and due to the long holding time some relaxation ("stress drop") is visible at stress state S3 (and also very minimal at stress state S2).

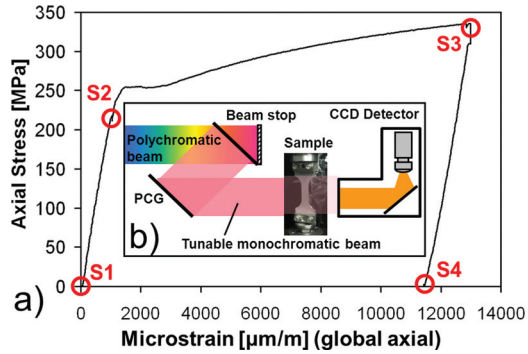

FIG. 2. (Color online) (a) Recorded stress-strain curve of tensile test. (b) Schematic sketch of CONRAD (inset).

The exact same type of sample (machined from the same batch) was used for measurements undertaken at the E3 Diffractometer (HZB). The tensile test has been performed with the same equipment and same parameters as at the CONRAD instrument, only but with more stress states being measured (12 stress states total, while the stress state at 90% of yield strength was measured twice). Several spatial locations along the specimen axis have been measured with a gauge volume of $2\times2\times2$ mm^3 while the count time for one point was 20 mins. The reader should note that the data presented herein was obtained for the (220) lattice plane, which represents lattice strains for the (110) lattice plane.

III. RESULTS

The (macroscopic) Poisson strain at the yield point (250 MPa) for the investigated material is 325 $\mu\varepsilon$, which corresponds to a Bragg peak shift of 0.0013 Å, while for engineering applications it is important to quantify strain with a precision of 50 to 100 $\mu\varepsilon$. To obtain the position of the Bragg edge for each pixel or spatial location, a curve routine was implemented using the nonlinear least-squares method. The derivative of the transmission profile was taken and a Gaussian fit applied, where the center of the Gaussian (A1) represents the location of the Bragg edge. (See Eq. (3))

$$f(x)=A_0e^{-[(x-A_1)/A_2]^2/2}+A_3 \tag{3}$$

In this notation, A_0 corresponds to the height of the Gaussian while A_2 is the width (standard deviation) of the Gaussian and A_3 stands for the constant term.

Based on the signal-to-noise ratio of intensity versus d-spacing data, the authors found it necessary to perform

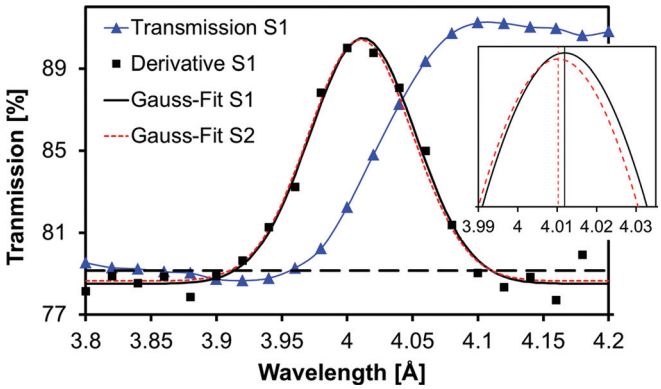

FIG. 3. (Color online) Bragg-edge transmission profile, derivative and gauss-fit.

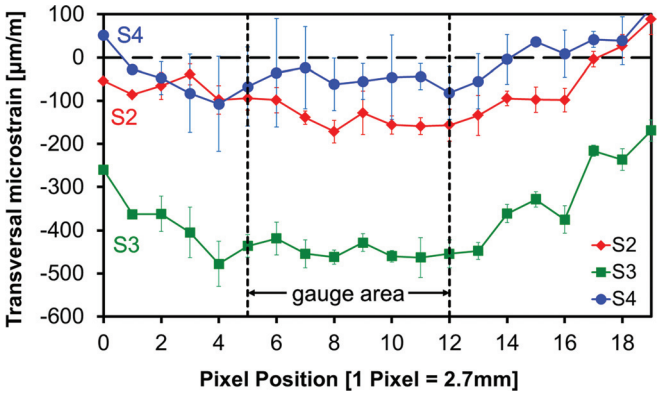

FIG. 5. (Color online) Transversal strains along the specimen height for investigated stress states.

additional spatial binning of pixels in order to determine the edge position with the required precision. This was necessary due to (relative) short exposure times implemented in our experiments to develop the measurement technique. By pixel binning the edges of the sample are spatially smeared out and a widening of the edge is introduced when binning pixels in the *y*-direction due to small wavelength variations along the height of the neutron beam. This is a known artifact of the double crystal monochromator setup and special care must be taken if the reference lattice parameter is obtained from a different sample (at a different position in the neutron beam path). The resulting pixel size was 2.7 mm, but longer count times and/or higher intensities are expected to lead to significant improvements of the spatial resolution possible with our technique. Also the thin specimen geometry, and therefore resulting thin diffracting gauge volume, should be noted.

The results show general agreement with expected strain values from elasticity theory and good agreement with experimental diffraction-based results, performed at the Residual Stress Analysis and Texture Diffractometer E3 at HZB, all within a variation of less than $\pm 60\mu\varepsilon$. Figure 3 shows the transmission profile for one pixel in the gauge center (2.7 mm pixel size after binning) as well as its derivative and fitted function for stress state S1. It also shows the fitted Gaussian curve for stress state S2 (dotted line) corresponding to the same pixel and the reader should note the shift of peak position (see also inset Fig. 3). The interpreted strain therefore is derived from the combination of measured experimental data and the approach identified in Eq. (3) for locating the peak position of different stress states. As is common with residual stress mapping facilities one can significantly improve the ability to measure d-spacing shifts much smaller than the available wavelength resolution $\Delta\lambda/\lambda$ with the option of using peak fitting technique. It is now routine that diffraction based instruments measure lattice strains smaller than 50 $\mu\varepsilon$. The reader should note that detectable d-spacing resolution is not defined just by wavelength band of the monochromator, but rather by the detectable diffraction peak (or shift of diffraction peak) of the sample.

The strain for each pixel, derived from the difference of the edge position in the stressed (S2, S3) and post-stressed condition (S4) to the unstressed condition (S1), is visualized in Fig. 4. One can note easily the differences between the stress states. The strains within the gauge area are uniform, while they are lower above and below it, corresponding to the tapered section. This is to be expected. Figure 5 presents the strains at the three stress conditions along the height of the specimen, pixel 0 corresponding to location at the bottom and pixel 19 at the top of the sample. Figure 6 compares transmission and diffraction-based results for the same location in the specimen center (while the diffracting gauge volume was chosen as $2 \times 2 \times 2$ mm^3). The error bars of the reported transmission data included in Figs. 5 and 6 correspond to two standard deviations of all horizontal pixels in the same line, which are expected to have the same strain due to plane stress condition. The determined strain values from both techniques agree with each other within the uncertainties of the experimental errors. A similar agreement was found in other locations along the specimen's height. The

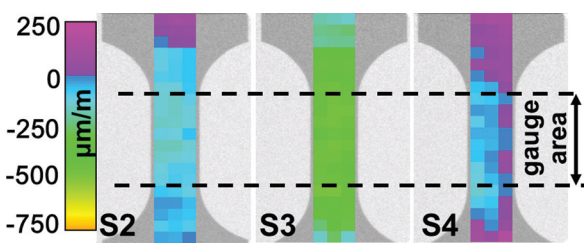

FIG. 4. (Color online) Map of transversal strains obtained by radiography.

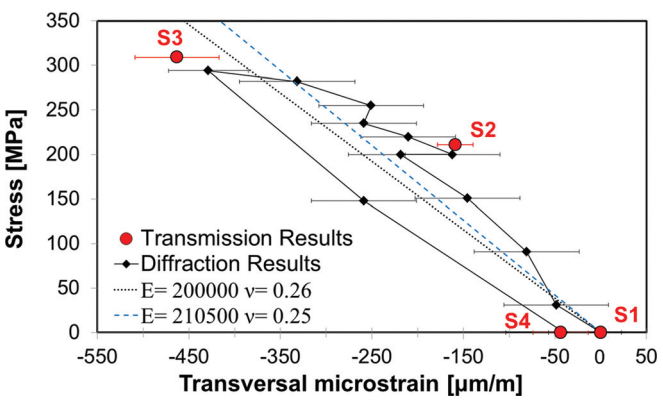

FIG. 6. (Color online) Comparison with diffractometer based results.

dotted black straight line indicates the macroscopic elastic response ($E = 200$ GPa, $\nu = 0.26$). It is expected from literature that the elastic response specific to the (110) plane of Fe^{α} behaves slightly different from that[32] ($E = 210.5$ GPa, $\nu = 0.25$; indicated by straight blue dashed line). The experimentally determined values at E3 lie within these expected values for applied stress magnitudes smaller than 90% of the yield point. The decrease of strain magnitude for the repeatedly measured stress state at 200 MPa could indicate that relaxation has occurred as more time has passed. This would also explain why the strain value of the transmission based result for stress S2 is relatively low, as the holding point has been even longer.

This work demonstrates first experiments that show the ability to do quantitative and spatially resolved strain radiography even with moderate fluxes at a reactor source. This technique could be useful for investigating typical plane stress problems using very small gauge volumes corresponding to pixel size and/or become a complementary tool for traditional diffractometers. It should be noted that the possibility of using very small gauge volumes is of course not only dependent on the technique itself, but also on the samples grain size, texture and microstructural properties. Moreover the technique can be applied to texture and phase analysis in the future. Future improvements leading to better spatial resolution and shorter count times are planned with improved monochromators and brighter sources.[33]

ACKNOWLEDGMENTS

The authors would like to thank Mr. K.G. Thomas (UTK) for manufacturing the loading system, samples and helpful discussions. Also appreciated is the support of Dr. A. Siriruk who performed complementary mechanical testing using a conventional MTS loading system. Dr. D. Penumadu would like to acknowledge the help from Drs. A. D. Krawitz and R. A. Winholtz who provided access to a portable uniaxial tensile testing system originally developed at University of Missouri.

[1]B. E. Allman, P. J. McMahon, K. A. Nugent, D. Paganin, D. L. Jacobson, M. Arif, and S. A. Werner, Nature **408**, 158 (2000).
[2]P. J. McMahon, B. E. Allman, D. J. Jacobson, M. Arif, S. A. Werner, and K. A. Nugent, Phys. Rev. Lett. **91**, 145502 (2003).
[3]N. Kardjilov, E. Lehmann, E. Steichele, and P. Vontobel, Nucl. Instrum. Methods Phys. Res. Sect. A **527**, 519 (2004).
[4]W. Treimer, M. Strobl, A. Hilger, C. Seifert, and U. Feye-Treimer, Appl. Phys. Lett. **83**, 398 (2003).
[5]M. Strobl, W. Treimer, and A. Hilger, Nucl. Instrum. Methods Phys. Res. Sect. B **222**, 653 (2004).
[6]F. Pfeiffer, C. Gruenzweig, O. Bunk, G. Frei, E. Lehmann, and C. David, Phys. Rev. Lett. **96**, 215505 (2006).
[7]M. Strobl, W. Treimer, P. Walter, S. Keil, and I. Manke, Appl. Phys. Lett. **91**, 254104 (2007).
[8]M. Strobl, C. Grünzweig, A. Hilger, I. Manke, N. Kardjilov, C. David, and F. Pfeiffer, Phys. Rev. Lett. **101**, 123902 (2008).
[9]C. Gruenzweig, C. David, O. Bunk, M. Dierolf, G. Frei, G. Kuehne, J. Kohlbrecher, R. Schaefer, P. Lejcek, H. M. R. Rønnow, and F. Pfeiffer, Appl. Phys. Lett. **93**, 112504 (2008).
[10]M. Strobl, W. Treimer, and A. Hilger, Appl. Phys. Lett. **85**, 488 (2004).
[11]N. Kardjilov, I. Manke, M. Strobl, A. Hilger, W. Treimer, T. Krist, and M. Meissner, Nature Phys. **4**, 399 (2008).
[12]M. Strobl, N. Kardjilov, A. Hilger, E Jericha, G. Badurek, I. Manke, Physica B **404**, 2611 (2009).
[13]M. Schulz, A. Neubauer, M. Mühlbauer, E. Calzada, B. Schillinger, C. Pfleiderer, and P. Böni, J. Phys.: Conf. Ser. **200**, 112009 (2010).
[14]M. Strobl, C. Pappas, A. Hilger, S. Wellert, N. Kardjilov, S. O. Seidel and I. Manke, "Polarized neutron imaging: A spin-echo approach," Phys. B, (in press).
[15]W. Treimer, M. Strobl, N. Kardjilov, A. Hilger, and I. Manke, Appl. Phys. Lett. **89**, 203504 (2006).
[16]N. Kardjilov, S. Baechler, M. Bastürk, M. Dierick, J. Jolie, E. Lehmann, T. Materna, B. Schillinger, and P. Vontobel, Nucl. Instrum. Methods A **501**, 536 (2003).
[17]A. Steuwer, P. J. Withers, J. R. Santisteban, L. Edwards, G. Bruno, M. E. Fitzpatrick, M. R. Daymond, M. W. Johnson, and D. Q. Wang, Phys. Status Solidi A **185**, 221 (2001).
[18]J. R. Santisteban, L. Edwards, A. Steuwer, and P. J. Withers, J. Appl. Cryst. **34**, 289 (2001).
[19]S. Vogel, Ph.D. thesis, Kiel University, 2000, available at http://e-diss.uni-kiel.de
[20]J. R. Santisteban, L. Edwards, M. E. Fitzpatrick, A. Steuwer, P. J. Withers, M. R. Daymond, M. W. Johnson, N. Rhodes, and E. M. Schooneveld, Nucl. Instrum. Methods A **481**, 765 (2002).
[21]J. R. Santisteban, L. Edwards, M. E. Fizpatrick, A. Steuwer, and P. J. Withers, Appl. Phys. A **74**, 1433 (2002).
[22]A. Steuwer, J. R. Santisteban, P. J. Withers, L. Edwards, and M. E. Fitzpatrick, J. Appl. Cryst. **36**, 1159 (2003).
[23]W. Kockelmann, G. Frei, E. H. Lehmann, P. Vontobel, and J. R. Santisteban, Nuclear Inst. Methods A **578**, 421 (2007).
[24]A. Steuwer, P. J. Withers, J. R. Santisteban, and L. Edwards, J. Appl. Phys. **97**, 074903 (2005).
[25]B. Abbey, S. Y. Zhang, and W. Vorster, Proc. Eng. **1**, 185 (2009).
[26]N. Kardjilov, A. Hilger, I. Manke, M. Strobl, M. Dawson, and J. Banhart, Nucl. Instrum. Methods Phys. Res. A **605**, 13 (2009).
[27]P. Boillat, D. Kramer, B. C. Seyfang, G. Frei, E. Lehmann, G. G. Scherer, A. Wokaun, Y. Ichikawa, Y. Tasaki, and K. Shinohara, Electrochem. Commun. **10**, 546 (2008).
[28]E. H. Lehmann, G. Frei, G. Kühne, and P. Boillat, Nucl. Instrum. Method Phys. Res. A **576**, 389 (2007).
[29]M. Strobl, I. Manke, N. Kardjilov, A. Hilger, M. Dawson, and J. Banhart, J. Phys. D: Appl. Phys. **42**, 243001 (2009).
[30]E. H. Lehmann, G. Frei, P. Vontobel, L. Josic, N. Kardjilov, A. Hilger, W. Kockelmann, and A. Steuwer, Nucl. Instrum. Methods A **603**, 429 (2009).
[31]M. Tamaki, Nucl. Instrum. Methods A **542**, 32 (2005).
[32]M. T. Hutchings, *Introduction to the Characterization of Residual Stress by Neutron Diffraction* (CRC Press, Boca Raton, FL, 2005).
[33]M. Strobl, Nucl. Instr. Methods A **604**, 646 (2009).